THz interferometric imaging using subwavelength plastic fiber based THz endoscopes

Ja-Yu Lu[1], Chung-Chiu Kuo[1], Chui-Min Chiu[1], Hung-Wen Chen[1], Yuh-Jing Hwang[2], Ci-Ling Pan[3], and Chi-Kuang Sun[1,4*]

[1]*Department of Electrical Engineering and Graduate Institute of Photonics and Optoelectronics, National Taiwan University, Taipei, 10617, Taiwan*
[2]*Institute of Astronomy & Astrophysics, Academia Sinica, Taipei, 10617, Taiwan*
[3]*Department of Photonics and Institute of Electro-Optical Engineering, National Chiao Tung University, Hsinchu, 30010, Taiwan*
[4] *Research Center for Applied Sciences, Academia Sinica, Taipei, 115, Taiwan*
[*]*Corresponding author: sun@cc.ee.ntu.edu.tw*

Abstract: We demonstrate a new reflective imaging technique using continuous-wave THz fiber-endoscopy, in which the sample is placed behind the output of a THz subwavelength plastic fiber and the Fabry Perot interference is formed therein. 3D THz reflective images with a reasonable SNR as well as high lateral and subwavelength axial resolutions are acquired by moving the sample along the axial (z) direction and by 2D scanning the output end of the subwavelength plastic fiber without any focusing medium. By analyzing the axial-position dependent THz signals backward collected by the subwavelength plastic fiber, the THz reflection amplitudes and phases on the sample surface can be successfully reconstructed.

OCIS codes: (110.2350) Fiber optics imaging; (300.6270) Spectroscopy, far infrared.

References and links

1. Y. Chen, H. Liu, Y. Deng, D. Veksler, M. Shur, and X.-C. Zhang, "Spectroscopic characterization of explosives in the far infrared region," SPIE Defense and Security Symp. #5411-2 (2004).
2. B. S. Ferguson, H. Liu, S. Hay, D. Findlay, X.-C. Zhang, and D. Abbott, "*In vitro* osteosarcoma biosensing using THz time domain spectroscopy," Proc. SPIE—Int. Soc. Opt. Eng. **5275**, 304 (2004).
3. K. McClatchey, M. T. Reiten, and R. A. Cheville, "Time resolved synthetic aperture terahertz impulse imaging," Appl. Phys. Lett. **79**, 4485–4487 (2001).
4. J. Pearce and D. Mittleman "Propagation of single-cycle terahertz pulses in random media," Opt. Lett. **26**, 2002 (2001).
5. R. A. Cheville, R.Wand. McGowan, and D. Grischkowsky, "Time resolved measurements which isolate the mechanisms responsible for terahertz glory scattering from dielectric spheres," Phys. Rev. Lett. **80**, 269 (1998).
6. K. Siebert, T. Loffler, H. Quast, M. Thomson, T. Bauer, R. Leonhardt, S. Czasch, and H. G. Roskos, "All-optoelectronic continuous wave THz imaging for biomedical applications" Phys. Med. Biol. **47**, 3743 (2002).
7. Siegel PH, Dengler RJ, "Terahertz heterodyne imaging Part II: Instruments" Int. J. Infrared Millimeter Waves **27**, 631 (2006).
8. A. Bandyopadhyay, A. Stepanov, B. Schulkin, M. D. Federici, A. Sengupta, D. Gary, J. F. Federici, R. Barat, Z. -H. Michalopoulou, and D. Zimdars, "Terahertz interferometric and synthetic aperture imaging," J. Opt. Soc. Am. A 23, 1168 (2006).
9. H.-W. Chen, J.-Y. Lu, L.-J. Chen, P.-J. Chiang, H.-C. Chang, Y.-T. Li, C.-L. Pan, and C.-K. Sun, "THz Fiber Directional Coupler," Proc. CLEO/QELS'2007, Baltimore, MD, USA (2007).
10. T.W. Crowe, W. L. Bishop, D. W. Porterfield, J. L. Hesler, and R. M. Weikle, "Opening the terahertz. window with integrated diode circuits," IEEE J. Solid States Circuits. **40**, 2104-2110 (2005).
11. J. E. Carlstrom, R. L. Plambeck, and D. D. Thornton, "A continuously Tunable 65-115 GHz Gunn Oscillator," IEEE Trans. Microwave Theory and Tech. **33**, 610-619 (1985).

#86933 - $15.00 USD Received 28 Aug 2007; revised 17 Oct 2007; accepted 22 Oct 2007; published 7 Feb 2008

12. J.-Y. Lu, C.-M. Chiu, C.-C.u Kuo, C.-H. Lai, H.-C. Chang, Y.-J. Hwang, C.-L. Pan, and Chi-Kuang Sun, "Terahertz scanning imaging with a subwavelength plastic fiber," revised version submitted to Appl. Phys. Lett..
13. B. Knoll, F. Keilmann, A. Kramer, and R. Guckenberger, "Contras of Microwave Near-field Microscopy," Appl. Phys. Lett. **70**, 2667-2669 (1997).
14. T. Taubner, F. Keilmann, and R. Hillenbrand, "Nanoscale-resolved subsurface imaging by scattering-type near-field optical microscopy," Opt. Express **13**, 8893-8899 (2005).
15. A. Tselev, S. M. Anlage, Z. Ma, and J. Melngailis, " Broadband dielectric microwave microscopy on micron length scales," Rev. Sci. Instrum. **78**, 044701 (2007).
16. D.M. Mittleman, M. Gupta, R. Neelamani, R.G. Baraniuk, J.V. Rudd, and M.Koch, "Recent advances in terahertz imaging," Appl. Phys. B **68**, 1085-1094 (1999).

1. Introduction

Many THz imaging and sensing techniques are under intense developments due to their sensitivity to molecular resonances. The most widespread method is the pulsed spectroscopic imaging based on the time-domain terahertz spectroscopy (TDTS) method, which enables the acquisition of a wide range of information including the absorption spectral characteristics [1,2], depth [3], and the nature of the scattered objects [4,5]. However, the optical components adopted in the pulsed imaging system are relatively large and expensive, while the TDTS system causes a small level of power per frequency. On the contrary, continuous-wave (CW) THz imaging systems are relatively compact, simple, and low-cost since they does not require a pump–probe time delay and thus the complexity of the optics involved can be greatly reduced [6]. For the requirement of broadband THz imaging, it could be addressed by using either multiple discrete frequencies or with a tunable source. Not only amplitudes, the phase information could also be retrieved in a CW THz imaging system through interferometric techniques [7,8].

In this work, we demonstrate THz fiber-based CW interferometric imaging. By using a subwavelength plastic fiber based THz endoscope, this reflective CW THz imaging system is capable of mapping both reflection amplitude and phase from the tested objects, corresponding to the molecular distribution and the depth profile. In the THz-fiber-endoscope, the sample to be imaged is placed close to the output of the imaging fiber and the Fabry Perot interference is formed between the sample surface and the output end of the fiber. 3D THz reflective images with a reasonable SNR and a high spatial resolution can be acquired by moving the sample along the axial (z) direction and by 2D lateral scanning the output end of the imaging fiber without any focusing medium. By analyzing the fiber-collected THz reflection signals for different sample axial positions, we can successfully reconstruct 3D THz images, which not only reflect the depth variation of the object surface but also reveal the reflectivity distribution recoupled back into the subwavelength fiber.

2. Experiment

The schematic diagram of the demonstrated THz fiber-endoscope is shown in Fig. 1(a). The THz fiber-endoscope was constructed with two THz subwavelength plastic fibers, which formed a fiber-based directional coupler [9]. The adopted highly flexible THz subwavelength polyethylene (PE) fibers were with a diameter of 240μm, while their measured attenuation constants at 320GHz were on the order of $9x10^{-3}$ cm^{-1}. 320GHz CW THz waves from a Gunn oscillator module [10,11] with a CW power level on the order of 350μW were coupled into and propagated along the input fiber (dot line) as shown in Fig. 1(a). By arranging part of these two fibers in parallel and touched each other as a directional coupler, a fraction of the input THz power will be coupled into the imaging fiber (solid line) through the overlapped region. The fiber directional coupler was constructed with the assist of two PE films on which a small hole was created for holding the two overlapped fibers together. The coupled THz waves transmitted along the straight imaging fiber were emitted from the fiber output end, reflected by the sample under test, and recoupled back along the same imaging fiber back to a

#86933 - $15.00 USD Received 28 Aug 2007; revised 17 Oct 2007; accepted 22 Oct 2007; published 7 Feb 2008

Golay cell (Microtech instruments) for detection. A chopper and a lock-in amplifier were used to improve the signal-to-noise-ratio (SNR). The transmitted THz power ratio at the outputs of the imaging and the input fibers was greater than 50 when the bending angles θ1 and θ2 (defined as shown in Fig. 1) were 37° and 7° respectively. Typically 20% of the incident THz power from the Gunn oscillator module could reach the object, after considering the propagation loss of a 90cm long fiber, the bending loss, and the input coupling and the directional coupling losses. The percentage of the reflected THz power collected and measured by the Golay cell was dependent on the reflectivity of sample and the re-coupling efficiency back to the subwavelength imaging fiber. For example, the 5% input THz power could be measured at the position of the Goley cell if a high reflectivity metal sample with a flat surface were adopted as the imaging object. By 2D lateral (x-y) scanning of the imaging-fiber output end around a spatially-fixed sample, a 2D THz fiber-endoscopic image could thus be obtained. Our previous study had indicated that within a scanning angle of ±2° , the fiber bending loss could be negligible [12]. The typical SNR of this imaging system is 1200:1 with a pixel dwelling time of 300 milliseconds. All the THz images shown in this work were acquired without normalized to the background, that is, we did not correct the angle-dependent bending loss.

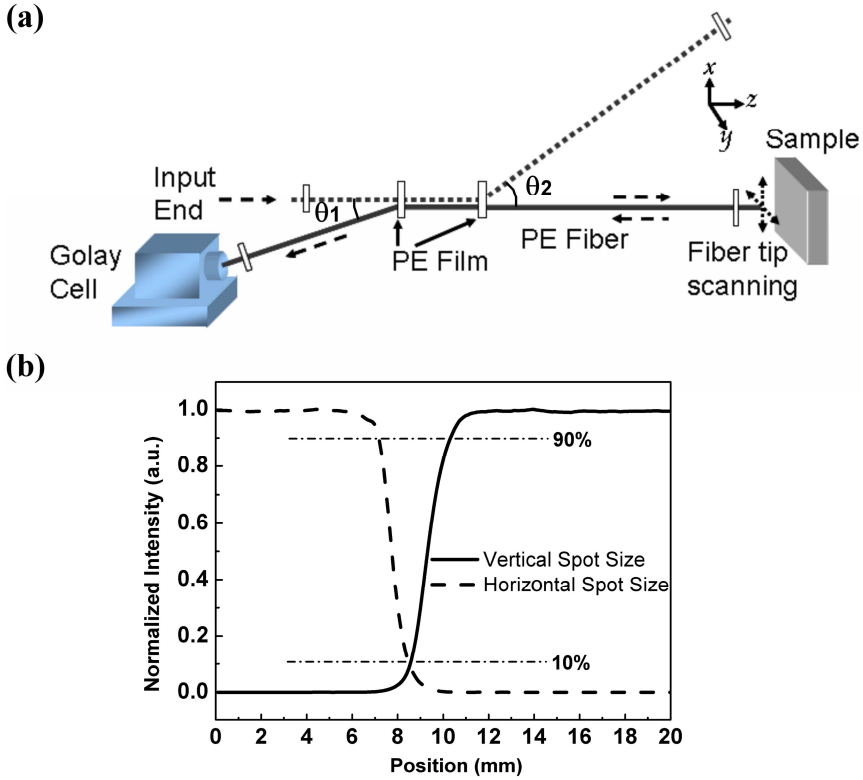

Fig. 1. (a) Schematic diagram of the THz fiber endoscope system based on two subwavelength plastic fibers. (b) The result of the THz spot size measurement.

Figure 1(b) shows the result of the THz spot size measurement (at 320GHz with a 938μm wavelength) performed at the output of the imaging fiber, by moving a sharp-edged metal blade, which was placed within 1mm in the z direction of the output end, across the output THz beam and by measuring the power after the metal-blade. The measured 10-90% power transmission distance was ~ 1.3mm, and the transmission curve was close to a circular transverse Gaussian mode. By fitting with a Gaussian spatial profile, a THz beam radius of

#86933 - $15.00 USD Received 28 Aug 2007; revised 17 Oct 2007; accepted 22 Oct 2007; published 7 Feb 2008

0.9 mm can be found, which revealed the fact that the subwavelength-fiber-based THz endoscope could reach a near-diffraction-limited lateral resolution within a near-field distance without focusing components. In addition, by moving the sample along the z direction versus the output end of the imaging fiber, we observed that the measured reflected THz power oscillated as shown in Fig. 2(a). This is due to the interference of multiple reflective THz waves between the sample surface and the output end of the imaging fiber. With this phenomenon we analyzed the phase information of the reflective THz waves, which is useful for providing the depth information of the THz image. In all our experiments, the distance between the imaging fiber tip and the sample tip was less than 5 mm. Even though the distance between the sample and the fiber tip was on the order of the wavelength, we did not observe obvious near field diffraction effect [13-15] in our experiments, due to the low numerical aperture value of the adopted sub-wavelength fiber. Our THz spot size measurement showed that the beam radius increase was less than 0.25 mm within the first 5 mm distance from the fiber tip.

3. Results and Discussion

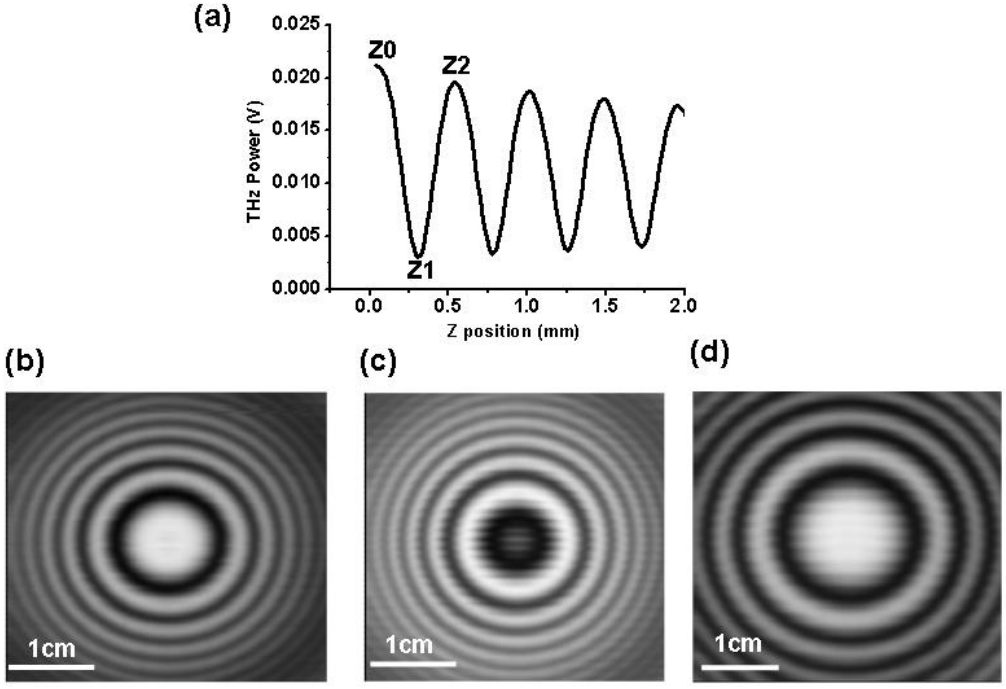

Fig. 2. (a) The Golay cell measured THz reflection power by moving the glass spherical lens 1 along the z direction away from the imaging fiber tip and by fixing the fiber-tip at the central point of the lens. (b) and (c) show the 2D fiber-scanning THz reflective images of the glass spherical lens 1 by positioning the lens at the fixed z0 and z1 positions respectively, as labeled in (a). (d) 2D fiber-scanning THz reflective images of the glass spherical lens 2 by positioning the lens at the fixed z0 position.

We first use two glass lenses as imaging objects to illustrate how we obtained the depth profile by utilizing the Fabry Perot interference pattern. By position the imaging fiber in the central point of the glass spherical lens 1 (with a focal length of 10cm) and by moving the lens along the z direction away from the fiber tip, Fig. 2(a) shows the Golay cell measured oscillatory THz reflection power due to the interference effect. The period of the Fabry Perot interference is 0.47mm (peak-to-peak), which is half of the adopted THz wavelength in air. By fixing the lens object at the z positions labeled as z0 or z1 in Fig. 2(a), we were able to

#86933 - $15.00 USD Received 28 Aug 2007; revised 17 Oct 2007; accepted 22 Oct 2007; published 7 Feb 2008

acquire 2D THz reflective imaging by moving the imaging fiber tip laterally. Thus acquired THz fiber-scanning images are shown in Fig. 2(b) and (c) with an image size of 32x32mm^2 and a fiber scanned step size of 0.16 mm in both x and y axes. Multiple rings are observed in the acquired 2D intensity images and these two images can be found to be out of phase with each other (bright rings become dark rings or vice versa). This result implies that the multiple rings come from the Fabry Perot effect, that is, the various z spacing between the curved lens surface and the fiber output end resulting in the observed constructive or destructive interference fringes. Figure 2(d) shows the 2D THz fiber-scanning reflective image of the glass lens 2 (with a focal length of 20cm) measured by positioning the lens tip at the fixed position z0. With a smoother surface profile of the glass lens 2, the reduced number of the observed oscillatory rings further confirms the fact that our images are sensitive to the Fabry-Perot effect. Based on the principle of the Fabry-Perot effect, we could thus analyze the surface profile of lens by comparing the 2D lateral scanning images acquired at different sample z positions within half of the THz wavelength (one oscillation cycle).

We then acquire various 2D THz fiber-scanning reflective images by moving the imaging object at different z positions within half of the THz wavelength to form a 3D data array. Our 3D image analysis is based on the assumption of a smooth surface profile. Without this assumption, phase ambiguity will occur. For example, the 2D fiber-scanned THz images shown in Fig. 2(b) ~ (d) contain two pieces of information from the samples. One is the surface profile (or depth distribution) and the other is the distribution of refractive index (including the real and imaginary parts) under the influence of the re-coupling efficiency. The depth information could be extracted by analyzing the z-dependent data with a fixed x-y position. We used a sinusoidal function to fit the z dependent intensity curves corresponding to different lateral positions just as in Fig. 2(a), and the fitting function was written as $y_i = \mathrm{A}\cos(k_z z_i + \phi_0) + C$, wherein A is the oscillation amplitude, $k_z = 2\pi/\lambda_z$ with λ_z as the period of oscillation (0.47mm), z_i is the sample z position, ϕ_0 is the initial phase that is not limited to be within 2π, and C is a constant. A and ϕ_0 were then extracted by minimizing the deviation $\Delta y_i^2 \equiv y^2 - y_i^2$, wherein y is the experimental data in the acquired 2D fiber-scanning THz images. The extracted oscillation amplitude A of the Fabry Perot interference represents the effective reflectivity distribution on the sample surface, which reflects the distribution of the refractive index (including absorption) in the measured THz frequency. The extracted initial phase ϕ_0 reflects the distance between the sample reflection surface and the imaging fiber tip. With a smooth surface assumption, the neighboring lateral (x-y) points are required to have minimum phase changes (height variations), thus avoiding the phase ambiguity. It should be noticed that with an inclined surface the recoupling efficiency will be modified, thus reducing the oscillation amplitude A while the initial phase ϕ_0 is not affected. Based on the correspondence between phase and distance at a specific x-y position, we were able to convert the extracted phases into heights and reconstruct the 3D surface profile with an axial resolution better than half of the wavelength.

Figure 3 (a) and (b) show the reconstructed 3D THz images of lens 1 and lens 2, in which colors represent different magnitudes of the extracted reflection oscillation amplitude A. With a glass-air interface, the decrease of the oscillation amplitude A from the center of the lens to its peripheral region supports our assumption that the oscillation amplitude A will be affected by the recoupling efficiency of the THz waves reflected from the curved surface back into the fiber. The reconstructed 3D surface profiles agree well with the lens maker formula (Fig. 4), indicating the accuracy of the phase extraction program. Even though the lens maker formula does not describe the exact curvature of the fabricated lens especially for the lens tip, the comparison in Fig. 4 indicates that the maximum inaccuracy of our phase retrieval program could be smaller than 0.15mm, supporting our hypothesis that our achieved axial resolution could be better than half of the applied THz wavelength.

#86933 - $15.00 USD Received 28 Aug 2007; revised 17 Oct 2007; accepted 22 Oct 2007; published 7 Feb 2008

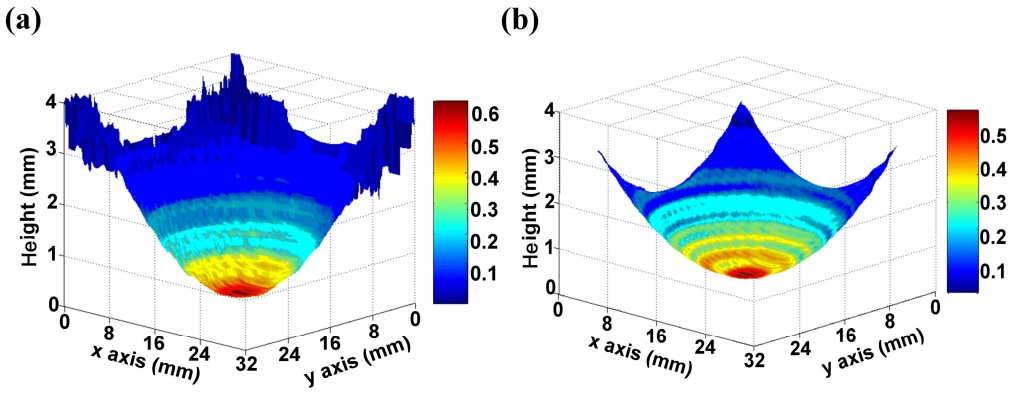

Fig. 3. Reconstructed 3D THz images of (a) lens 1 and (b) lens 2. Colors represent different magnitudes of the extracted reflection oscillation amplitude A. These images were acquired by the THz interferometric fiber-endoscope.

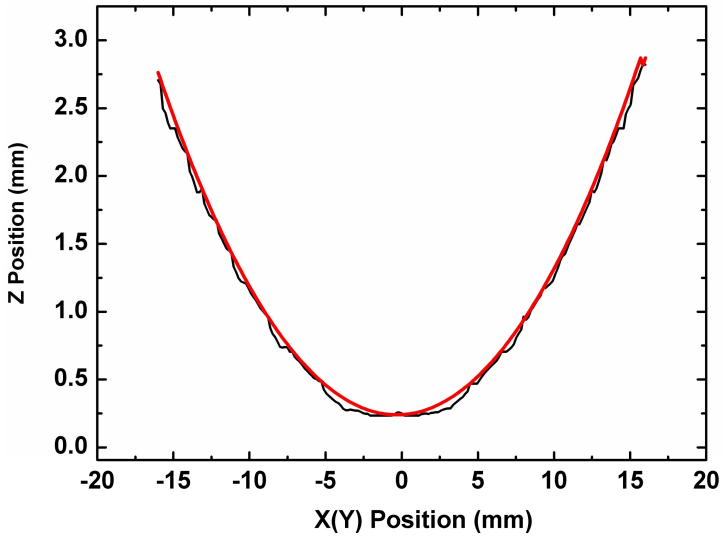

Fig. 4. Reconstructed surface profile (black line) of lens 1 and its comparison with the lens maker formula (red line).

We then apply our developed fiber-endoscopy for biological THz imaging, such as the diagnosis of burned skin. A porcine skin purchased from the market was first burned by a heated iron tube with an outer diameter of 1cm and then fixed on a stage for THz fiber endoscopic imaging. The THz fiber-endoscopy imaging was performed with an axial and a lateral scanned step size of 0.08mm and 0.4mm respectively. In this preliminary test we first scanned the fiber to complete a 2D lateral image with a size of 32X16 mm^2 and with a pixel dwelling time of 300 milliseconds, and then moved the z stage for another lateral scan. With a z step size of 0.08 mm, we found that only 6 axial positions are required to complete our analysis, corresponding to one oscillation circle. Figure 5(a) and (b) show the THz 2D images corresponding to the extracted amplitude A and phase ϕ_0 from the burned porcine skin, and (c) is the reconstructed 3D THz image of the burned porcine skin. Similar to Fig. 3 (a) and (b), we adopt different colors to represent different reflection oscillation amplitudes A. The smooth surface profile assumption was used to avoid the phase ambiguity during the extraction process. In Fig. 5(a) and (c), the reflection oscillation amplitude A at the ring-

#86933 - $15.00 USD Received 28 Aug 2007; revised 17 Oct 2007; accepted 22 Oct 2007; published 7 Feb 2008

shaped burned area can be found to be smaller than other parts of skin. This could not be simply explained by the inclined surface but should also be contributed from the strongly reduced THz reflection, especially at the bottom of the burned area. This THz reflectivity reduction could be attributed to the much-reduced water content in the burned area, which is consistent with a previous report [16]. It is interesting to notice that from Fig. 5(c), the lateral resolution of the system can be found to be around 1mm, which was limited by the beam radius of the emitted THz beam after the fiber tip, rather than the lateral scanned step size, which was smaller than half of the beam radius.

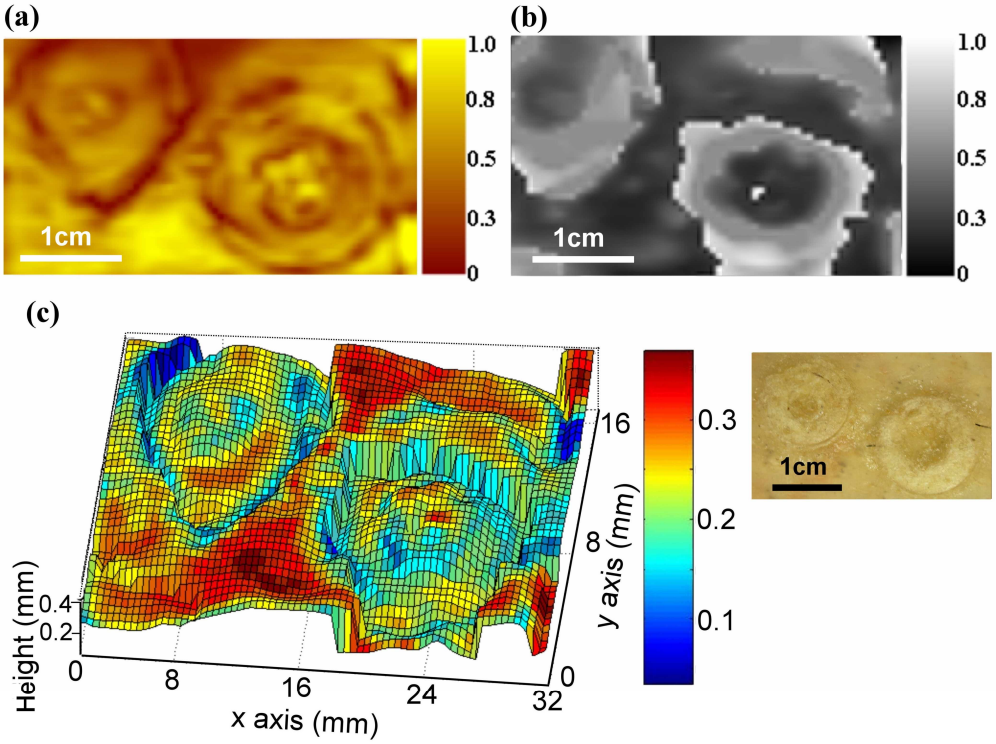

Fig. 5 THz 2D image corresponding to the (a) extracted amplitude A and the (b) phase ϕ0 from the burned porcine skin. The ring-shaped burned area can be clearly identified. (c) The reconstructed 3D THz image of the burned porcine skin. Colors represent the extracted reflection oscillation amplitude A. This image was acquired by the THz interferometric fiber-endoscope. Inset shows the photo of the burned porcine skin. The THz reconstructed image matches well with the optical image.

4. Conclusion

In conclusion, we have demonstrated THz interferometric imaging by using a subwavelength-plastic-fiber-based THz endoscope. The reflective THz images with a subwavelength axial resolution, a reasonable SNR, and a high lateral resolution (near diffraction limit) were acquired by moving the sample along the axial (z) direction and by 2D scanning the output end of the subwavelength plastic fiber without any focusing system. The reconstructed 3D images not only reflect the depth variation of the object surface, but also reveal the THz reflectivity distribution recoupled back into the subwavelength fiber. By improving the acquisition time with a fast THz detector in the future, this demonstrated THz system could open the possibility of medical endoscopic molecular imaging.

#86933 - $15.00 USD Received 28 Aug 2007; revised 17 Oct 2007; accepted 22 Oct 2007; published 7 Feb 2008

Acknowledgement

This work was sponsored by the National Science Council of Taiwan under grants 96-2628-E-002-043-MY3 and 96-2120-M-002-014, Frontier Research of National Taiwan University 95R0110, the Program for Promoting Academic Excellence of University Project (Phase II) in National Chiao Tung University, National Health Research Institute of Taiwan NHRI-EX96-9201EI, and the NTU Research Center For Medical Excellence.

#86933 - $15.00 USD Received 28 Aug 2007; revised 17 Oct 2007; accepted 22 Oct 2007; published 7 Feb 2008